Journal of Applied Fluid Mechanics, Vol. 17, No. 3, pp. 713-725, 2024.
Available online at www.jafmonline.net, ISSN 1735-3572, EISSN 1735-3645.
https://doi.org/10.47176/jafm.17.3.2056

Effect of the Guide Vane on the Hydraulic Stability of a Low-head, Large-discharge Industrial Hydraulic Turbine

L. Xue[1], B. Cui[1], Z. Zhu[1], R. Wang [2], Z. Yang [3], J. Hu[1] and X. Su[1†]

[1] *State-Province Joint Engineering Lab of Fluid Transmission System Technology, Zhejiang Sci-Tech University, Hangzhou, 310018, China*
[2.] *Xinjiang Tianfu Energy Sales Power Co. LTD, Shihezi, Xinjiang, 832000, China*
[3.] *Xinjiang Tianfu Environmental Protection Technology Co., LTD, Shihezi, Xinjiang, 832000, China*

†Corresponding Author Email: suxianghui@zstu.edu.cn

ABSTRACT

The hydraulic turbine has been used extensively in the field of energy conservation. For turbines that have low heads and large discharge, improving recovery efficiency and stability is crucial due to their significant hydraulic impact. This paper provides a detailed analysis of the correlation between the influence of radial guide vanes on the stability of low-head, large-discharge turbines focusing on hydraulic performance and energy dissipation before and after the implementation of guide vanes. Moreover, in this paper, two types of turbines, with and without guide vanes, were designed considering the desulfurization scenario. Hydraulic efficiency, radial force, and internal flow field mechanics were numerically studied, and validated through experiments. The results reveal that the working range of the hydraulic turbine could be widened and the energy recovery efficiency improved by a maximum of 3.11% in the small flow rate under the action of guide vanes. Furthermore, it results in a substantial reduction in the radial force of the impeller. Subsequently, the variation in entropy production of different components under full flow rate conditions was compared between the models with and without guide vanes. The total energy consumption decreases sharply under overall working conditions due to the flow control ability of guide vanes affecting the flow state. The entropy production rate of the impeller remains the largest regardless of the presence of a guide vane in the turbine. The vortices inside the guide vanes increase obviously with the flow rate increase.

Article History

Received June 7, 2023
Revised October 15, 2023
Accepted October 17, 2023
Available online January 1, 2024

Keywords:

Guide vane
Low-head and large-discharge
Hydraulic turbine
Hydraulic stability
Entropy generation rate
Vortex characteristics

1. INTRODUCTION

In recent years, increasing attention has been given to clean energy and energy recovery due to the growing demand for energy consumption. Turbines, as core equipment, have been widely adopted in various application. For example, turbines are used in water supply systems for urban freshwater pipelines (Carravetta et al., 2017; Du et al., 2017; Lydon et al., 2017), micro-hydro power schemes in remote area power supply and energy recovery systems (Polák, 2021; Lu et al., 2022), pumped storage hydro for energy storage techniques (Giosio et al., 2015), and pressure regulation and recovery devices in water systems for deep mines (Van Antwerpen & Greyvenstein, 2005). Small and medium-sized non-traditional hydro turbines are widely used for energy recovery; however, most studies focus on single-stage pump as turbine (PAT) systems. However, single-stage PAT systems have power recovery and efficiency limitations. Derakhshan & Nourbakhsh (2008) derived established relationships based on experimental data to predict the best efficiency point of a pump operating as a turbine according to the pump's hydraulic characteristics. Based on laboratory results, Pugliese et al. (2016) studied the performance of pumps working in reverse mode. Venturini et al. (2018) developed a physics-based new simulation model to predict the performance characteristics of PATs according to the performance curves of the original pump. Moreover, Huang et al. (2017) introduced an innovative theoretical approach and predicted the flow rate and head at the best efficiency point for both pump and turbine. This approach was verified to be more accurate through experimental results. Jain et al. (2015) assessed the effect of modification parameters on improving the hydraulic performance of the PAT at different working conditions. The results revealed that simultaneous modification of parameters in the off-design condition reduces losses while increasing efficiency and power generation. Wang et al. (2017) designed a dedicated impeller with forward-curved blades and significantly improved the performance of the PAT.

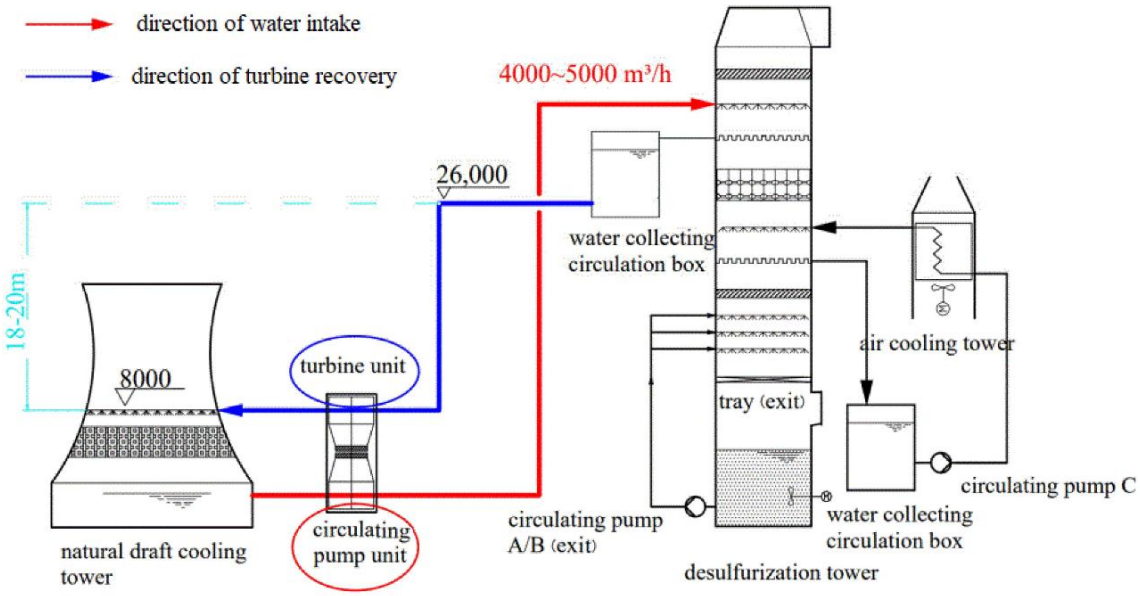

Fig. 1 Turbine in desulfurization tower (Su et al., 2021)

While double-discharge hydraulic turbines offer high recovery efficiency, they also generate excessive radial forces due to the large hydraulic impact, an urgent issue that needs to be addressed. Adding radial guide vanes has been verified as an effective method to address the problem of excessive radial force in single-stage PATs and centrifugal pumps. Shi et al. (2018) investigated the effects of different guide vane numbers on the unsteady performance of single-stage PAT. Qian et al. (2016) evaluated the performance of an axial-flow pump with adjustable guide vanes in turbine mode, and they found that the adjustable guide vanes play an important role in improving the efficiency of the axial-flow PAT and reducing costs under partial loading. Zhang et al. (2022) provided an available energy recovery method for the double-discharge turbine used in desulfurization, which was a novel contribution.

However, there is limited reported research on the influence of guide vanes on double-discharge hydraulic turbines. In this study, two low-head and large-discharge hydraulic turbines, with and without guide vanes were designed for a ship desulfurization energy recovery system, as illustrated in Fig.1. The influence of guide vanes on hydraulic stability was systematically studied considering the external characteristics, internal flow field features and energy loss. Recently, the mechanisms of entropy generation theory have been used as essential references for analyzing energy dissipation in pumps and turbines through numerical methods (Gong et al., 2013; Ghorani et al., 2020; Zhang et al., 2020; Lin et al., 2021; Xu et al., 2022; Yu et al., 2022; Zeng et al., 2022; Zhou et al., 2022). These methods have been verified to be more precise and convenient than traditional pressure dropping methods through comparative of experiments. Ghorani et al. (2020) conducted a numerical investigation on the mechanisms of energy loss in a PAT based on entropy generation theory to obtain the quantity of energy dissipation and the exact location. Tang et al. (2022) reported that numerical simulation and experiments yielded similar results for hydraulic performances. Yu et al. (2022) adopted a modified turbulence model to obtain the energy loss locations along the pump-turbine passage under different working conditions. Zhang et al. (2020) evaluated the energy losses in a side channel pump at different wrapping angles by the entropy generation method and obtained the exact regions of high hydraulic losses. As previously reported, adding guide vanes between the impeller and the volute is an effective optimization to improve the drainage capacity of volute. Overall, the entropy generation method will be adopted in this study to obtain the energy loss characteristics of the turbines.

In summary, this article supplies a novel and feasible optimization scheme for low-head and large-discharge energy recovery devices to broaden the range of turbine's applications.

2. MATHEMATICAL MODEL AND NUMERICAL METHOD

2.1 Entropy Production Theory

The energy dissipation theory was introduced to analyze the energy loss in this industrial hydraulic turbine, wherein there is increasing entropy during energy exchange. The entropy generation can be explored in a fluid machine system based on the second law of thermodynamics. Generally, the inner fluid of the turbine is incompressible, moreover, the heat transfer is not considered. The entropy production rate mainly consists of viscous dissipation and turbulence dissipation, represented by$S_{\overline{D}}$ and $S_{D'}$ respectively. $S_{\overline{D}}$ and $S_{D'}$ can be calculated directly through numerical simulation using the following Eqs. (1) and (2):

$$S_{\overline{D}} = \frac{\mu}{T}\left[\left(\frac{\partial \overline{v}}{\partial x}+\frac{\partial \overline{u}}{\partial y}\right)^2+\left(\frac{\partial \overline{w}}{\partial x}+\frac{\partial \overline{u}}{\partial z}\right)^2+\left(\frac{\partial \overline{v}}{\partial z}+\frac{\partial \overline{w}}{\partial y}\right)^2\right]+ 2\frac{\mu}{T}\left[\left(\frac{\partial \overline{u}}{\partial x}\right)^2+\left(\frac{\partial \overline{v}}{\partial y}\right)^2+\left(\frac{\partial \overline{w}}{\partial z}\right)^2\right] \quad (1)$$

$$S_{D'} = \frac{\mu}{T}\left[\left(\frac{\partial v'}{\partial x}+\frac{\partial u'}{\partial y}\right)^2+\left(\frac{\partial w'}{\partial x}+\frac{\partial u'}{\partial z}\right)^2+\left(\frac{\partial v'}{\partial z}+\frac{\partial w'}{\partial y}\right)^2\right]+$$

$$2\frac{\mu}{T}\left[\left(\frac{\partial u'}{\partial x}\right)^2+\left(\frac{\partial v'}{\partial y}\right)^2+\left(\frac{\partial w'}{\partial z}\right)^2\right] \quad (2)$$

Here, μ represents the dynamic viscosity (Pa s), T represents the temperature (K) and u, v and w represent the velocity components (m/s). The entropy generation rate $S_{D'}$ generated in the $k-\omega$ turbulent model can be replaced by Eq. (3):

$$S_{D'} = \beta\frac{\rho k\omega}{T} \quad (3)$$

Here, β is a constant equal to 0.09, k, ω and ρ represent the turbulent kinetic, dissipation rate of the turbulent kinetic energy and density (kg/m^3), respectively.

The total entropy generation rate (EGR) can be obtained with Eq. (4):

$$S_D = S_{\overline{D}} + S_{D'} \quad (4)$$

The total EGR S_{pro} is obtained by integrating $S_{\overline{D}}$ and $S_{D'}$ on the corresponding fluid domain Eq. (5) as follows:

$$S_{pro} = \iiint_V (S_{pro,\overline{D}} + S_{pro,D'})dV \quad (5)$$

2.2 Design of Radial Guide Vane

A low-head, large-discharge hydraulic turbine is used to recover the high-pressure in an optimised desulfurization water circulation system. This turbine is studied as physical Model A with a head size of 6.5 m and a designed flow rate of 1200 m^3/h. To elucidate the stability correlation of how guide vanes impact the hydraulic turbine, the other structure with guide vanes is marked as Model B. Detailed numerical and experimental studies were performed based on models A and B. Guide vanes usually provide a better angle to match the incoming flow and reduce the flow dissipation. The magnitude of velocity circulation at the trailing edge of a guide vane can be deduced through the velocity triangle as indicated in Fig. 2.

The circumferential velocity of the fluid within the guide vane is obtained using the following equation:

$$V_u = V_r\cot\alpha = \frac{Q}{2\pi R b_3}\cot\alpha \quad (6)$$

Here, α is the installation angle of the guide cane blade, R is the distance from the point to the center of rotation; and b_3 is the thickness of the guide vane blade. Therefore, the velocity circulation of the fluid at the inlet and outlet of the guide vane can be expressed as follows:

$$\Gamma_0 = 2\pi R_0 V_{0u} = \frac{Q}{b_3}\cot\alpha_0 \quad (7)$$

$$\Gamma_1 = \frac{Q}{b_3}\cot\alpha_1 \quad (8)$$

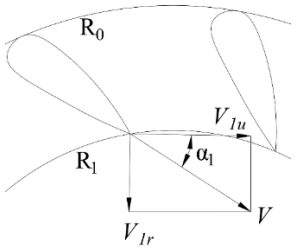

Fig. 2 Velocity triangle of guide vane

During the hydraulic design of the volute component, the velocity circulation Γ_0 at the inlet of the guide vane is equal to that at the outlet of the liquid flow in the volute Γ', and the relation is as follows:

$$\Gamma' = 2\pi K_2 = \Gamma_0 = \frac{Q'}{b_3}cot\,\alpha_0 \quad (9)$$

According to Eqs. (7-9), the inlet placing angle of the guide vane α_0 can be obtained.

The velocity circulation along a closed curve in a flow field equals the sum of the velocity circulations passing through any surface bounded by the curve. This is based on applying Stokes' theorem used in fluid mechanics. In other words, the velocity circulation at the inlet of the guide vane Γ_0 equal to the sum of the velocity circulation at the outlet Γ_1 and the velocity circulation between blade passages Γ_Z. as presented in Eq. (10):

$$\Gamma_0 = \Gamma_Z + \Gamma_1 \quad (10)$$

The velocity circulation between blade passages Γ_Z can be calculated using the following Eq. (11):

$$\Gamma_Z = \frac{\Gamma_0 - \Gamma_1}{Z} \quad (11)$$

According to the formula, it can be obtained that the velocity circulation of the liquid flow into the impeller can be changed by adjusting the placement angle of the guide vane. In this study, the specific speed of the hydraulic turbine is low and the structure of the volute is large. This causes the velocity circulation of the liquid flow at the outlet of the guide vane to be insufficient in providing sufficient energy for the impeller to rotate. Therefore, the inlet angle of guide vane is designed to be greater than the outlet angle and to be increase the velocity circulation of the outlet liquid flow accordingly.

Considering that no external force is acting on the liquid flow in the transition interval from the guide vane outlet to the impeller inlet, the velocity circulation will not change. Thus, the velocity circulation at the impeller inlet is equal to the velocity circulation formed at the outlet of the guide vane. According to the hydrodynamic momentum equation of the hydraulic turbine, it can be obtained as follows:

$$H\eta_h = \frac{\omega}{2\pi g}(\Gamma_1 - \Gamma_3) \quad (12)$$

Therefore, the circumferential component of the liquid flow velocity at the point before the guide vane outlet is derived using Eq. (13):

Table 1 Geometric parameters of Model A and B

Domain	Parameter	Model A	Model B
Impeller	Inlet diameter of the inlet D_1	410 mm	410 mm
	Outlet diameter of the inlet D_2	300 mm	300 mm
	Blade number Z	6	6
Volute	Inlet diameter D_3	350 mm	350 mm
	Outlet diameterD_7	410 mm	560 mm
	Outlet width b_2	236 mm	236 mm
Suction chamber	Inlet diameter (D_4)	300 mm	300 mm
	Outlet diameter (D_5)	450 mm	450 mm
Guide vane	Diameter of distribution circle	/	354 mm
	Blade number	/	11
	Outlet diameter (D_7)	/	560 mm
	Inlet placement Angle (α_0)	/	27°
	Outlet placement Angle (α_d)	/	23.5°

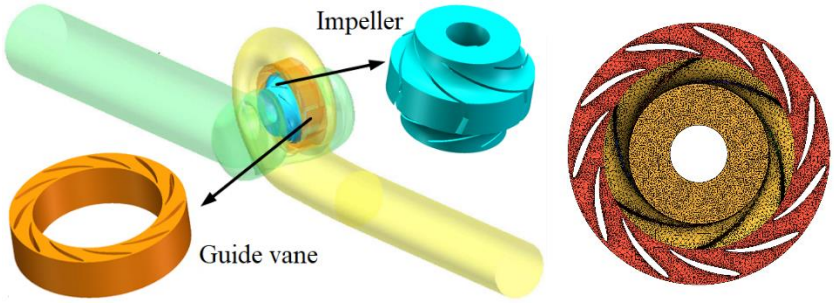

(a) (b)

Fig. 3 Simulation domain of Model B and grids of the impeller and guide vane

$$V'_{1u} = \frac{gH\eta_h + \Gamma_3\omega}{\omega r'_1} \tag{13}$$

It is generally believed that the outlet placing angle α_d of the guide vane is equal to the liquid flow angle α'. The liquid flow angle is obtained through Eq. (14):

$$\tan\alpha'_1 = \frac{Q\omega}{2\pi b_3\psi_1(gH\eta_h + \frac{w\Gamma_3}{2\pi})} \tag{14}$$

Here, η_h is the turbine efficiency; ω is the angular velocity of the impeller and Γ_3 is the velocity circulation at the outlet of the impeller. Since the outlet of the double suction-turbine's two impellers is the normal outlet, the theoretical circumferential velocity of the impeller outlet is 0. Therefore, the outlet ring quantity is zero. ψ_1 represents the exclusion coefficient of the guide vane. The critical parameter for determining the placing angle of the outlet in the guide vane can be obtained.

The double-discharge hydraulic turbine impeller has six unilateral blades. To reduce the resonance phenomenon that affects system stability, the number of guide vanes is selected to be greater than that of the impeller. The detailed geometric parameters of Models A and B are listed in Table 1.

Model A consists of three calculation domains: volute, impeller and suction chamber. Model B includes an additional guide vane. To minimize the influence of boundary conditions on the calculation domains, extensions five times the diameter are added at the inlet of the volute and the outlet of the discharge tube. Fig.3(a) displays the simulation domain of Model B.

2.3 Numerical Procedure

Considering the superior adaptability of unstructured grids, this calculation model is divided into unstructured. The verification of mesh independence, as shown in Fig. 4(a), indicates that efficiency surpasses the limitations imposed by the number of meshes, and the efficiency fluctuation is small when the number of mesh exceeded nearly 14 million in Model A and 15 million in Model B. The detailed mesh information selected in this article is listed in Table 2. Due to the high-velocity gradient near-wall, a fine grid resolution is required for the near-wall

Table 2 Grid information for each part

Components	Number of grids (Model A)	Number of grids (Model B)
Inlet extension	650,760	650,760
Volute	5,460,480	5,832,650
Impeller	6,285,570	6,285,570
Guide vane	/	986,433
Suction chamber	1,104,239	1,104,239
Outlet extension	706,430	706,430

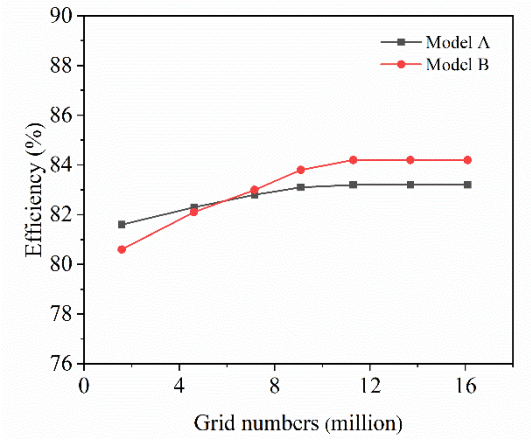

(a)

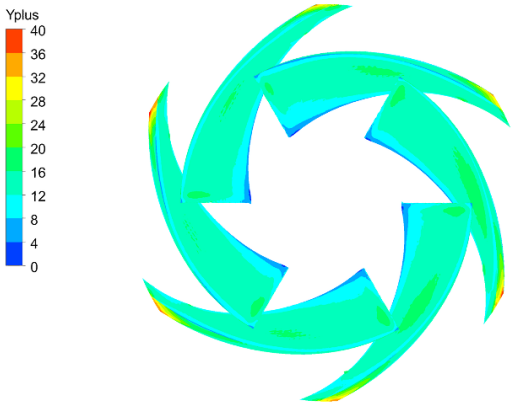

(b)

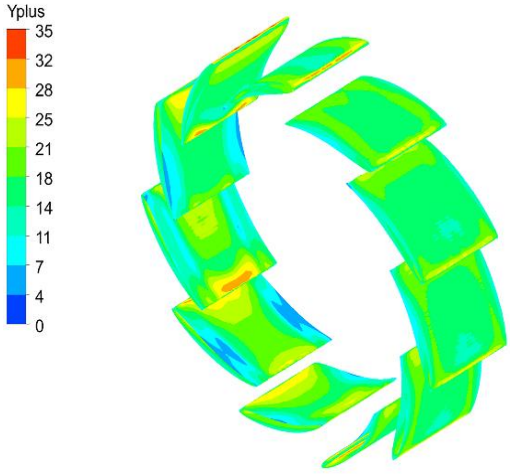

(c)

Fig. 4 Grid independence verification: (a) Models A and B (b) distribution of y plus on blade in Model B and (c) distribution of y plus on guide vane in Model B

area. Y plus which represents the non-dimensional wall distance is necessary to be considered. Fig.4(b) and 4(c) display the values of y plus on the impeller and guide vanes which indicate that the maximum values of the blade and guide vane do not exceed 40; moreover, the main values range from 5-20. The mesh of the impeller and guide vane in Model B is displayed in Fig.3(b)and 3(c).

Table 3 Boundary conditions

Working point	Model A	Model B
Impeller rotation speed (rpm)	580	580
Inlet total pressure (kPa)	300	300
Mass flow outlet(kg/s)	333.33	333.33

CFX 18.2 was employed for unsteady numerical calculations in this study due to the reliability and accuracy in solving the fluid dynamic problems for complicated geometric models. This paper selects water at 25℃ as the working fluid. The SST$k-\omega$ model is chosen for the simulations, and all walls in Models A and B are set as non-slip walls. Table 3 indicates the boundary conditions of Models A and B working under design point. The calculation finished when the convergence error was less than 10^{-5}. By adjusting the outlet flow, different turbine characteristics could be obtained.

3. EXPERIMENTAL VALIDATION

An experimental platform displayed in Fig.6 has been built to verify the reliability of the numerical simulation in this research. Fig. 6(a) depict the turbine test rig, and Fig.6(b) shows the turbine test system. The energy in the high-pressure water supplied by the feed pump is transferred to the turbine. The coupler connects the load pump and the turbine to adjust the speed of the load pump accordingly. Valve 2 is adopted to change the pressure and flow rate at the turbine inlet while valve 3 is used to control the outlet pressure of the turbine. The outlet pressure and flow rate of the load pump are regulated by changing valve 4. Moreover, the flow rate of the turbine and the load pump is measured by flow meters 1 and 2, respectively. The pressure at the inlet and outlet of the hydraulic turbine is measured by pressure transmitters 1 and 2. The measuring ranges and accuracy of the test devices are displayed as Table 4. Through the method of "square, sum and root", the uncertainty of flow rate, head, shaft power and efficiency in this experimental system are respectively ±1.22%, ±1.05%, ±2.08% and ±2.64%.

Before starting the experiment, the air in the turbine pipeline is exhausted to ensure that there is no air interference in the pipeline by closing valves 1, 3 and 4. The following steps show the detailed operating flows;

(1) Valve 4 at the outlet of the load pump is kept unchanged, valve1 is turned off. The feed pump is started and valve 2 is gradually open. After the turbine runs to the designed speed, the inlet and outlet pressure, flowrate and torque are monitored and recorded when the operation is stable.

(2) Increase the opening of valve 2, then the flow rate、pressure、torque and other parameters of the turbine at the same speed are obtained by adjusting valve 4 at the outlet of the load pump.

(3) Repeat the above step to obtain turbine performance at different flow points at the designed speed. When the flow rate of the feed pump is too large and the head is insufficient, valve 1 on the bypass is opened

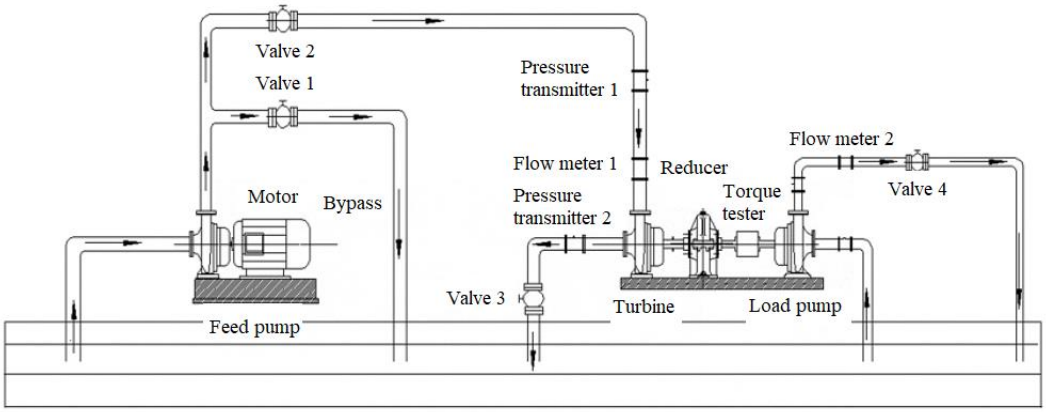

(a)

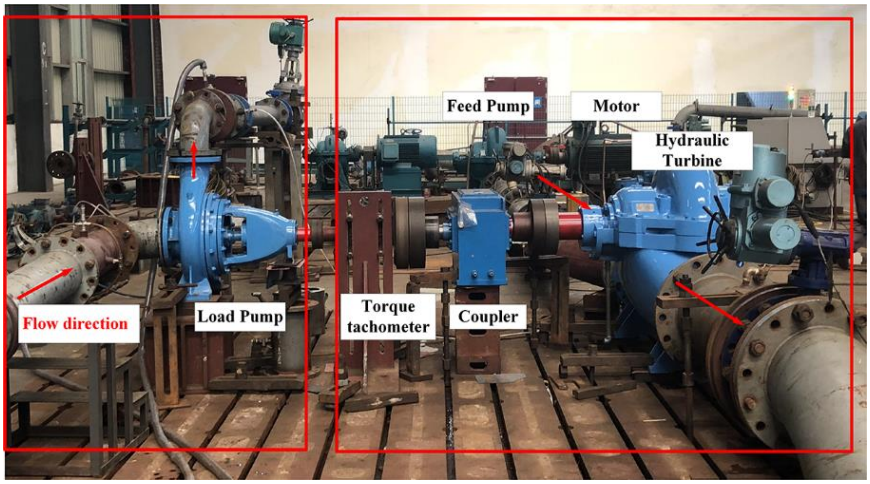

(b)

Fig. 6(a) Schematic of turbine test rig and (b) turbine test system

Table 4 Information of measurement apparatus

Measurement apparatus	Range	Accuracy (%)
Flow meter1	0.1~10 m^3/s	±0.5
Flow meter2	0.1~10 m^3/s	±0.5
Pressure transmitter 1	0~1MPa	±0.1
Pressure transmitter 2	−300~300 kPa	±0.1
Torque tester	0~500 Nm	±0.3
Speed tester	0~13000rpm	±0.01

(4) to further obtain turbine performance parameters at other flow points at required speed.

(5) Finally, the full characteristic curve of the turbine at designed speed can be obtained.

4. RESULTS AND DISCUSSIONS

4.1 Hydraulic Characteristic and Radial Force

The performance of head and efficiency obtained via simulation in Model A concurs with that from the experimental test shown in Fig.7, which indicates the accuracy of the numerical calculation. The simulation results are higher than that obtained from experimental test because of the leakage losses and surface roughness are not considered. The head and efficiency in Models A and B are similarly observed under overall conditions. Adding a guide vane profile increases the efficiency under

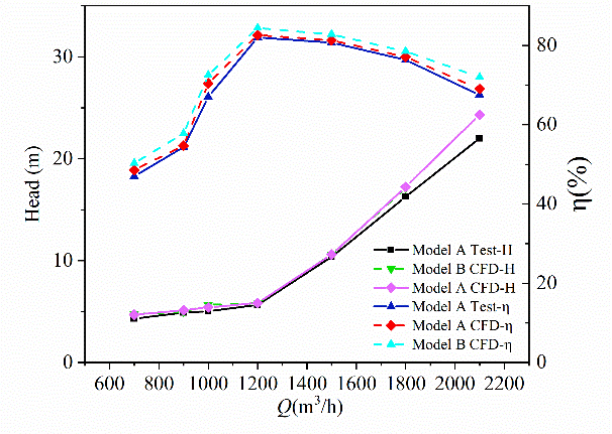

Fig. 7 Performance of head and efficiency by CFD method and simulation between Models A and B

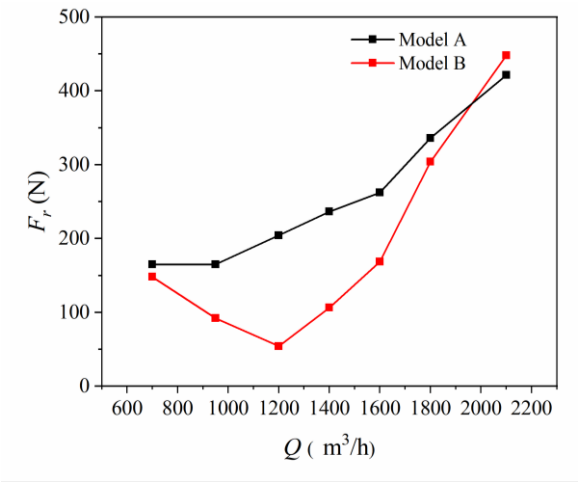

Fig. 8 Radial force of Models A and B

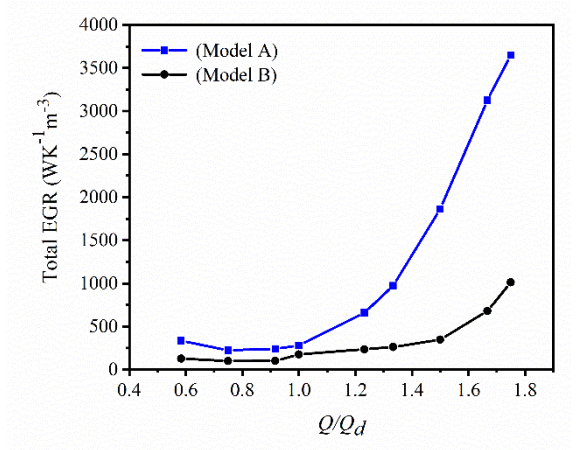

Fig. 9 Comparison of total EGR in Models A and B at different flow rate

partial conditions. The efficiency improves from 82.6% to 84.4% at the design flow rate, while the maximum efficiency improvement is 3.11% at 900 m^3/h. Therefore, it can be concluded that the increase in the guide vane profile broadens the working range of the low-head and large-discharge hydraulic turbine, and improves efficiency under overall conditions.

The radial force of the impeller is the resultant force superimposed by the horizontal and vertical components of the fluid pressure load acting on the impeller. Fig.8 shows the proper distribution of radial forces for the two models under different working conditions. The radial force in each working condition in Model B is smaller than that of Model A except for the flow rate at 2100 m^3/h. This phenomenon indicates that the guide vanes rectify the liquid flow before entering the impeller, making the liquid flow into the impeller as evenly as possible.

4.2 Energy Generation Rate Characteristics

The total EGR under different flow rates were compared for Models A and B to obtain the energy dissipation, as shown in Fig.9. The trend of the total EGR curve is similar, with the largest EGR occurring at the highest flow rate. Moreover, the total EGR in Model A

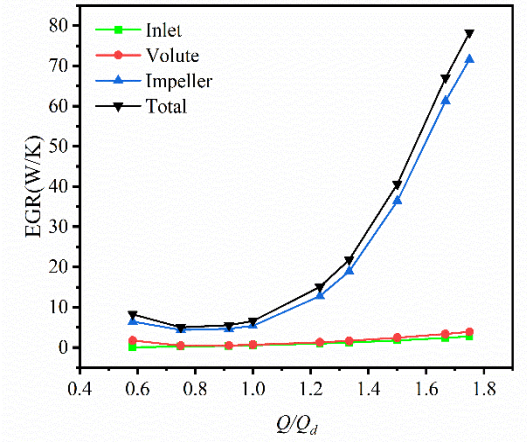

(a)

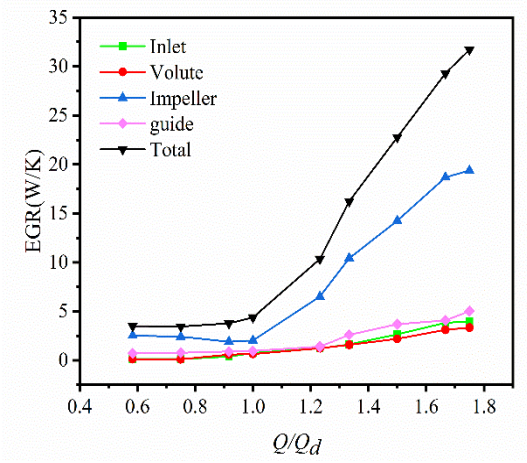

(b)

Fig. 10 Entropy production power of each component in (a) Model A and (b) Model B

under the same working condition is always higher than that of Model B, due to the addition of the guide vane profile. Figure10 demonstrates the entropy production power of each component, indicating that the entropy production of both Models A and B initially decreases slowly and then gradually increases with the flow rate increases. When the flow rate is close to the design condition（Q_d）, the entropy production of this turbine drops to its lowest point, which is 1.073 kW in Model A and 3.7 kW in Model B.

For the detailed study of energy loss, the average EGR under different flow rates of each component for Models A and B is depicted in Fig.11. Overall, the EGR in the impeller is the largest which aligns with Fig.9. When the flow rate increases, the EGR also increases. When the flow rate is 1.75 times the design flow rate, the EGR of the impeller is almost 70 W/K in Model A but sharply reduces to 18.7 W/K in Model B. Therefore, using the guide vane effectively reduces energy loss in components in Model B. The proportion of energy loss in each component to the total energy loss of Models A and B is shown in Fig.12. The EGR proportion of the impeller relative to the whole turbine ranges from 78 to 91% at different flow rates in Model A and reduces to 46 to 72% in Model B accounting for majority of the total EGR.

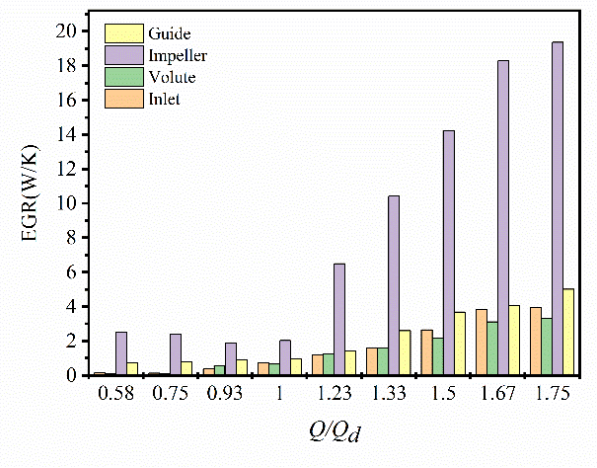

(a)

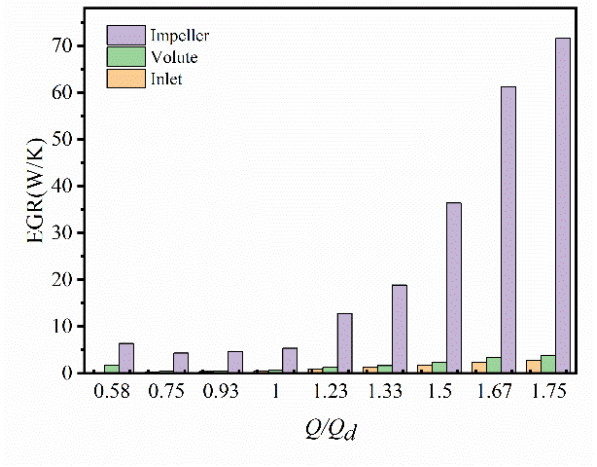

(b)

Fig. 11 Total EGR of different components at different flow rates in (a) Model A and (b)Model B

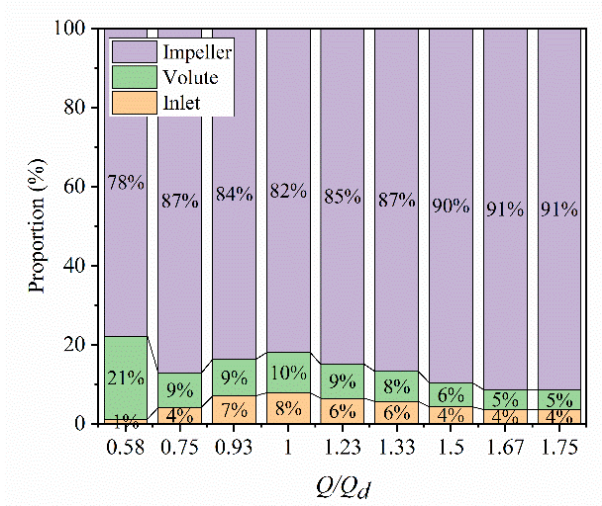

(a)

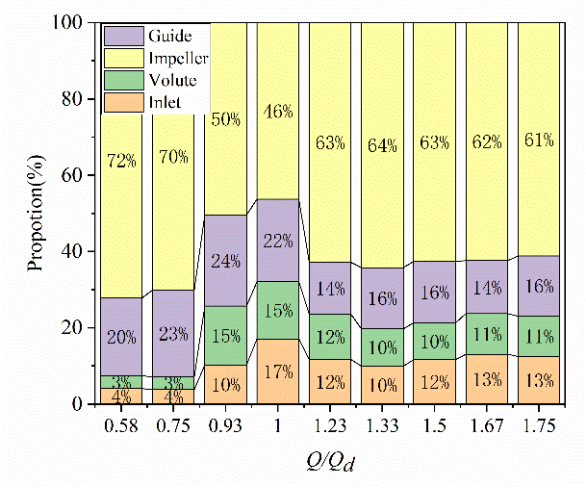

(b)

Fig. 12 Proportion of each component energy loss in the total energy loss in (a) Model A and (b) Model B

According to the analysis above, it is vital to investigate the energy loss of the impeller in detail to optimize the hydraulic performance of the turbine. Fig.13 shows the distribution of volume-averaged entropy production and streamlines in the impeller of Models A and B under different flow rates. The high hydraulic loss is mainly concentrated in the middle and outlet of the impeller passage in Model A at a large discharge of 2100 m^3/h. Meanwhile, the streamlines indicate that the large velocity gradient induces vortices that block the entire blade section passage. The streamlines are almost smooth under the designed flow rate, corresponding to a low entropy production rate. When the flow rate is reduced to 700 m^3/h, all the high EGR regions move to the blade trailing edge due to flow deviation and the mismatch between the flow outlet angle in the volute and the blade inlet angle. Compared with Model A, the entropy production rate in Model B is obviously decreased at overall flow rates, while the overall tendency is similar. At a large flow rate of 2100 m^3/h, vortices can still be observed in the velocity streamline distribution, but they are noticeably smaller, which can explain the steep downwards trend of the impeller's EGR. When the flow rate is reduced to 700 m^3/h, as indicated in Fig.14, number of vortices decreases significantly due to the important role played by the guide vane in adjusting the flow before entering the impeller, which reduces the flow impact. Another reason is that the velocity is not high and the influence of turbulence is minimal. In summary, the vortices in the blade passage and the leading edge of the impeller disturb the flow stability of the turbine in Model A under partial conditions. With the addition of guide vanes, the flow stability improved, correspondingly, the performance of the turbine improved.

Figure 15 describes the volume-averaged entropy distribution on the horizontal section of the volute under different flow rates in Models A and B. The largest entropy production is obtained at the outlet of the volute under the lowest flow rate conditions. The entropy generation intensity and hydraulic losses in these regions decrease significantly, reaching their lowest value under the designed condition. A large flow rate intensifies regions with a remarkably high local EGR around the volute walls when the flow rate reaches 2100 m^3/h. This is because the upstream fluid cannot smoothly enter the flow channel. Eventually, the fluid enters the impeller after merging with the downstream fluid. However, in Model B, the entropy generation in the volute is sharply reduced and moves towards the outlet of the guide vane in overall

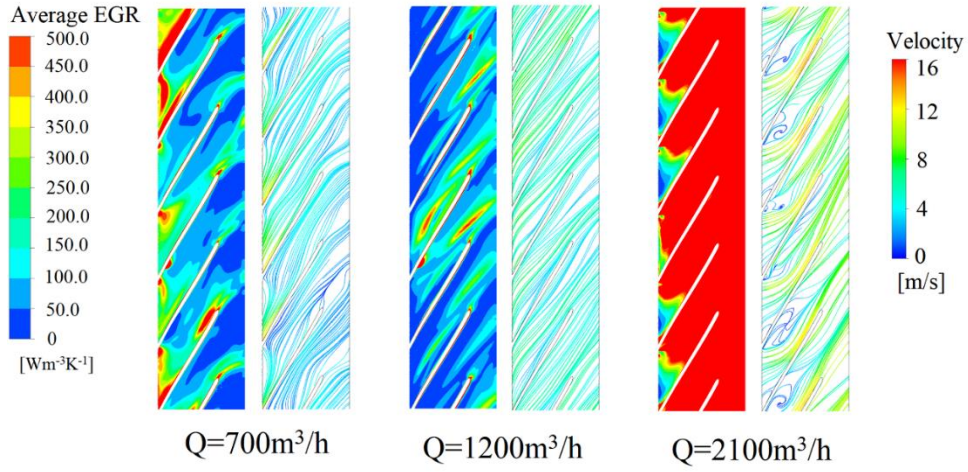

(a)

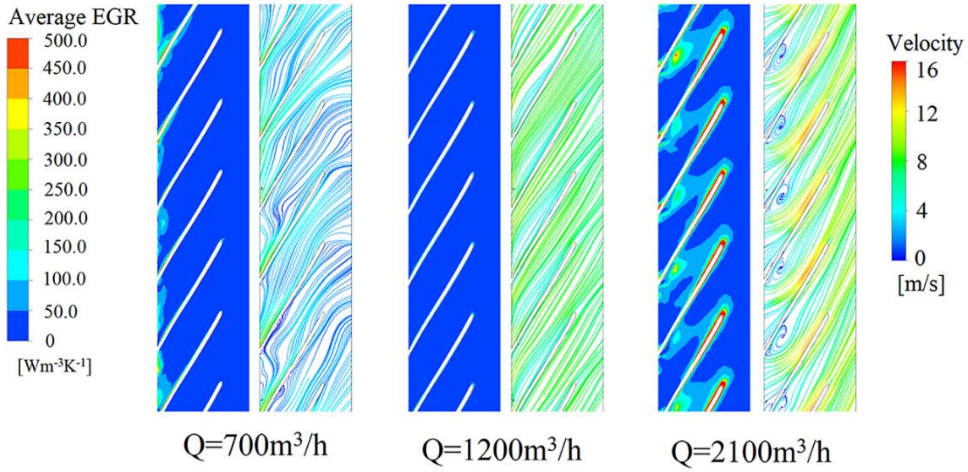

(b)

Fig. 13 Average volume EPR distribution and streamlines in different spanwise surfaces in impeller (a) Model A and (b) Model B

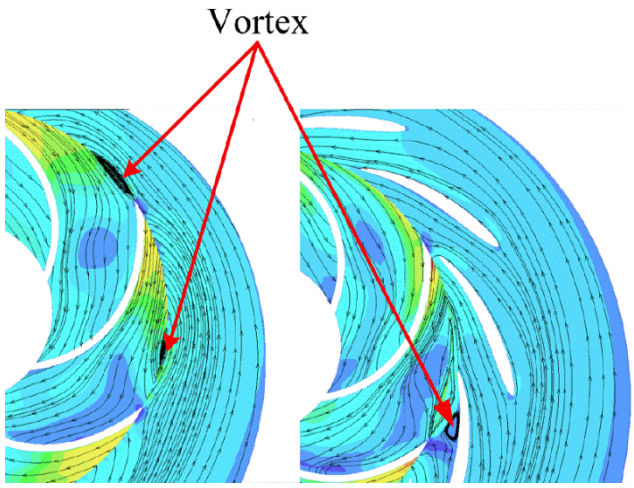

Fig. 14 Contour of velocity at 700 m^3/h in Model A and Model B

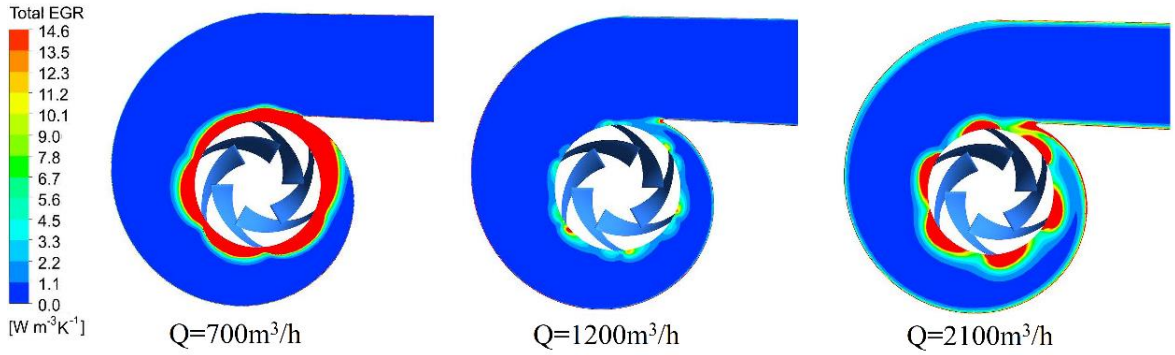

(a)

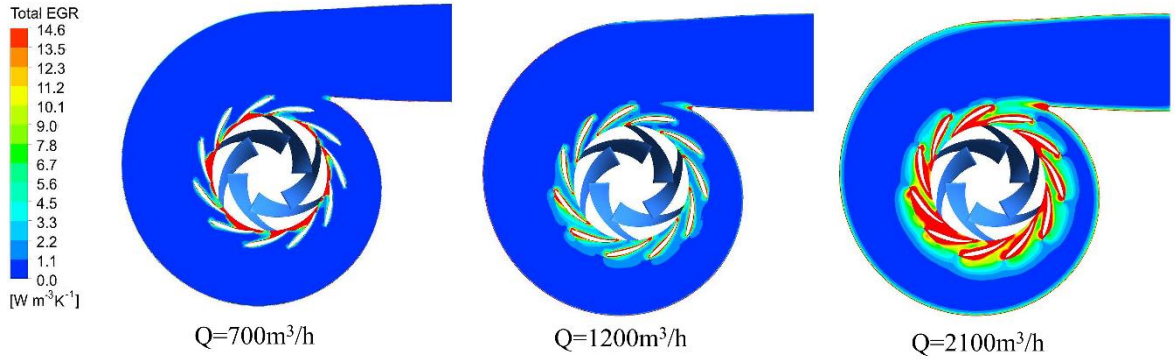

(b)

Fig. 15 Volume averaged EGR distribution in volute and guide vane in (a) Model A and (b) Model B

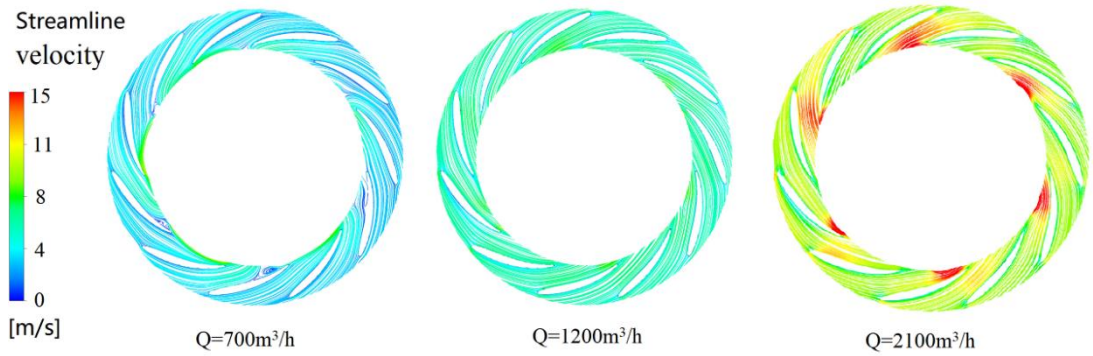

(a)

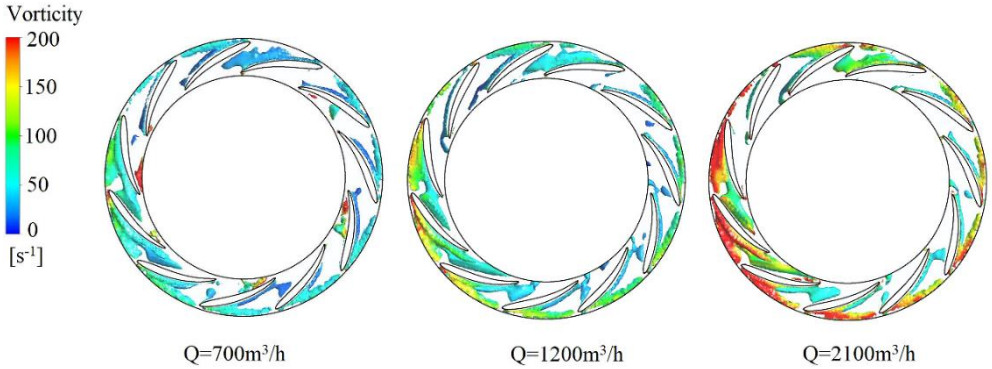

(b)

Fig. 16 Streamline velocity and vortex distribution of guide vane under different flow rates

conditions. The region with high energy loss reduces significantly under a small flow rate of 700 m^3/h. Under design conditions, the EGR is much lower than the other two working conditions. Under a large flow condition of 2100 m^3/h, the EGR is mainly concentrated at the outlet of the volute in Model A and near the outlet of the guide vane in Model B. Compared with Model A, the guide vane in Model B ensures smoother flow, leading to a sharp decrease in entropy dissipation. Notably, the casing tongue region has consistently been a location of noticeable losses. In conclusion, the guide vane effectively reduces energy consumption, making it a suitable approach to investigating EGR depth.

4.3 Flow Features in Guide Vane

Vortex is a typical flow feature in hydraulic machinery, which induces various instability problems, such as strong pressure pulsation, high noise, vibration, rotating stall, cavitation erosion, and material fatigue (Zhang et al., 2018a, b; Liu et al., 2019; Qian et al., 2022; Xu et al., 2022). To further elucidate the influence of the guide vane on the flow field in the double-discharge turbine, the flow features in the guide vane under design flow conditions are studied combination with the omega vortex model. Fig.16 illustrates the guide vane's streamline and omega vortex distribution under different flow conditions when the threshold is 0.72. The results show that the streamline in the guide vane at different flow rates is almost smooth. The velocity increases gradually from the inlet to the outlet along the flow passage of the guide vane under full operation conditions and reaches the maximum value at the outlet of the guide vane with the largest flow rate of 2100 m^3/h. Fig.16(b) shows the vortices distribution on the surface of the guide vane. The vortices are commonly concentrated at the inlet of the guide vane and reduce sharply in the flow direction, indicating that the guide vane structure makes the liquid flow regular. It is observed that the vortices inside the guide vane increase with the increase in flow rate.

5. CONCLUSIONS

This research systematically analyzes the energy evolution characteristics and internal flow field features of a low-head and large-discharge hydraulic turbine before and after the addition of a guide vane using numerical and experimental methods. The effects of the guide vane on the stability of the hydraulic turbine are as follows:

(1) Applying the guide vane profile improves the turbine's overall efficiency. The improvement effect is more pronounced in extreme flow conditions, which widens the high-efficiency working range of the turbine.

(2) The impeller accounts for the largest entropy production in the turbine. Adding the guide vane substantially reduce the entropy production of the impeller and volute under overall working conditions. Additionally, the guide vane optimizes the flow capacity of the liquid in the channel, resulting in reduced energy dissipation.

(3) The velocity circulation inside the guide vane increases with the flow rate. The vortex is typically concentrated at the inlet of the guide vane and diminishes significantly in the flow direction.

In summary, the guide vane improves the stability of the hydraulic turbine and expands the high-efficiency working conditions, which is important for optimized design methods. In future studies, more attention should be paid to the relationship between the geometrical parameters of the guide vane and the turbine's performance in specific operations to broaden its applications.

ACKNOWLEDGEMENTS

This work was supported by The Joint Funds of the National Natural Science Foundation of China (Grant No. U2006221), Key Research and Development Program of Zhejiang Province (No. 2023C04034) and Major science and technology projects of the Science and Technology Department of Xinjiang Construction Corps (No. 2021AA002).

CONFLICT OF INTERESTS

The author declare that they have no known competing financial interests or personal relationships that could have appeared to influence the work reported in this paper.

AUTHOR CONTRIBUTIONS

Ling Xue: Software, Investigation, Writing-original draft; **Baoling Cui**: Writing - review & editing; **Zuchao Zhu**: Conceptualization, Methodology; **Runsheng Wang**: Software, Validation; Zhiguo Yang: Software, Validation; **Jianxin Hu**: Software, Validation; **Xianghui Su**: Writing - review & editing, Supervision

REFERENCES

Carravetta, A., Antipodi, L., Golia, U., & Fecarotta, O. (2017). Energy Saving in a water supply network by coupling a pump and a pump as turbine (PAT) in a turbopump. *Water*, *9*(1). https://doi.org/10.3390/w9010062

Derakhshan, S., & Nourbakhsh, A. (2008). Experimental study of characteristic curves of centrifugal pumps working as turbines in different specific speeds. *Experimental Thermal and Fluid Science*, *32*(3), 800-807. https://doi.org/10.1016/j.expthermflusci.2007.10.004

Du, J., Yang, H., Shen, Z., & Chen, J. (2017). Micro hydro power generation from water supply system in high rise buildings using pump as turbines. *Energy*, *137*, 431-440. https://doi.org/10.1016/j.energy.2017.03.023

Ghorani, M. M., Sotoude Haghighi, M. H., Maleki, A., & Riasi, A. (2020). A numerical study on mechanisms of energy dissipation in a pump as turbine (PAT) using entropy generation theory. *Renewable Energy*, *162*, 1036-1053. https://doi.org/10.1016/j.renene.2020.08.102

Giosio, D. R., Henderson, A. D., Walker, J. M., Brandner, P. A., Sargison, J. E., & Gautam, P. (2015). Design and performance evaluation of a pump-as-turbine micro-hydro test facility with incorporated inlet flow

control. *Renewable Energy*, *78*, 1-6. https://doi.org/10.1016/j.renene.2014.12.027

Gong, R., Wang, H., Chen, L., Li, D., Zhang, H., & Wei, X. (2013). Application of entropy production theory to hydro-turbine hydraulic analysis. *Science China Technological Sciences*, *56*(7), 1636-1643. https://doi.org/10.1007/s11431-013-5229-y

Huang, S., Qiu, G., Su, X., Chen, J., & Zou, W. (2017). Performance prediction of a centrifugal pump as turbine using rotor-volute matching principle. *Renewable Energy*, *108*, 64-71. https://doi.org/10.1016/j.renene.2020.08.109

Jain, S. V., Swarnkar, A., Motwani, K. H., & Patel, R. N. (2015). Effects of impeller diameter and rotational speed on performance of pump running in turbine mode. *Energy Conversion and Management*, *89*, 808-824. https://doi.org/10.1016/j.enconman.2014.10.036

Lin, T., Li, X., Zhu, Z., Xie, J., Li, Y., & Yang, H. (2021). Application of enstrophy dissipation to analyze energy loss in a centrifugal pump as turbine. *Renewable Energy*, *163*, 41-55. https://doi.org/10.1016/j.renene.2020.08.109

Liu, J. M., Gao, Y. S., Wang, Y. Q., & Liu, C. (2019). Objective omega vortex identification method. *Journal of Hydrodynamics*, *31*(3), 455-463. https://doi.org/10.1007/s42241-019-0028-y

Lu, Z., Xiao, R., Tao, R., Li, P., & Liu, W. (2022). Influence of guide vane profile on the flow energy dissipation in a reversible pump-turbine at pump mode. *Journal of Energy Storage*, *49*. https://doi.org/10.1016/j.est.2022.104161

Lydon, T., Coughlan, P., & McNabola, A. (2017). Pressure management and energy recovery in water distribution networks: Development of design and selection methodologies using three pump-as-turbine case studies. *Renewable Energy*, *114*, 1038-1050. https://doi.org/10.1016/j.renene.2017.07.120

Polák, M. (2021). Innovation of Pump as turbine according to calculation model for francis turbine design. *Energies*, *14*(9). https://doi.org/10.3390/en14092698

Pugliese, F., De Paola, F., Fontana, N., Giugni, M., & Marini, G. (2016). Experimental characterization of two Pumps As Turbines for hydropower generation. *Renewable Energy*, *99*, 180-187. https://doi.org/10.1016/j.renene.2016.06.051

Qian, B., Cai, Y., Ding, Q., Zhao, D., Sun, W., & Wang, L. (2022). Investigation of tip leakage vortex structure and trajectory in a centrifugal pump with a new omega vortex identification method. *Applied Sciences*, *12*(10). https://doi.org/10.3390/app12105270

Su, X., Cao, Z., Li, Y., Jin, Y., & Tang, Z. (2021). Research on flow stability and vibration of an industrial hydraulic turbine. *Processes*, *9*(2). https://doi.org/10.3390/pr9020311

Shi, F., Yang, J., & Wang, X. (2018). Analysis on the effect of variable guide vane numbers on the performance of pump as turbine. *Advances in Mechanical Engineering*, *10* (6), https://doi.org/10.1177/1687814018780796

Tang , X., Jiang,W., Li,Q., Gao, Y., Zhang, N.,Wang, Y., & Chen, D. (2022). Analysis of hydraulic loss of the centrifugal pump as turbine based on internal flow feature and entropy generation theory. *Sustainable Energy Technologies and Assessments*, *52*.

https://doi.org/10.1016/j.seta.2022.102070

Van Antwerpen, H. J., & Greyvenstein, G. P. (2005). Use of turbines for simultaneous pressure regulation and recovery in secondary cooling water systems in deep mines. *Energy Conversion and Management*, *46*(4), 563-575. https://doi.org/10.1016/j.enconman.2004.04.006

Venturini, M., Manservigi, L., Alvisi, S., &Simani, S. (2018). Development of a physics-based model to predict the performance of pumps as turbines. *Applied Energy*, *231*, 343-354. https://doi.org/10.1016/j.renene.2022.06.077

Wang,T., Kong, F., Xia, B., Bai, Y., & Wang, C. (2017). The method for determining blade inlet angle of special impeller using in turbine mode of centrifugal pump as turbine. *Renewable Energy*, *109*, 518-528. https://doi.org/10.1016/j.renene.2017.03.054

Xu, L., Guo, T., & Wang, W., (2022). Effects of Vortex structure on hydraulic loss in a low head francis turbine under overall operating conditions base on entropy production method. *Renewable Energy*, *198*, 367-379. https://doi.org/10.1016/j.renene.2022.08.084

Yu, A., Li, L., Ji, J., & Tang, Q. (2022). Numerical study on the energy evaluation characteristics in a pump turbine based on the thermodynamic entropy theory. *Renewable Energy*, *195*, 766-779. https://doi.org/10.1016/j.renene.2022.06.077

Zeng, H., Li, Z., Li, D., Chen, H., & Li, Z. (2022). Vortex distribution and energy loss in s-shaped region of pump turbine. *Frontiers in Energy Research*, *10*. https://doi.org/10.3389/fenrg.2022.904202

Zhang, F., Appiah, D., Hong, F., Zhang, J., Yuan, S., Adu-Poku, K. A., & Wei, X. (2020). Energy loss evaluation in a side channel pump under different wrapping angles using entropy production method. *International Communications in Heat and Mass Transfer*, *113*. https://doi.org/10.1016/j.icheatmasstransfer.2020.104526

Zhang, Y., Liu, K., Li, J., Xian, H., & Du, X., (2018a). Analysis of the vortices in the inner flow of reversible pump turbine with the new omega vortex identification method. *Journal of Hydrodynamics*, *30*(3), 463-469. https://doi.org/10.1007/s42241-018-0046-1

Zhang, Y., Liu, K., Xian, H., & Du, X. (2018b). A review of methods for vortex identification in hydroturbines. *Renewable and Sustainable Energy Reviews*, *81*, 1269-1285. https://doi.org/10.1016/j.rser.2017.05.058

Zhang, Z., Su, X., Jin, Y., Zhu, Z., & Lin,T. (2022). Research on energy recovery through hydraulic turbine system in marine desulfurization application.

Sustainable Energy Technologies and Assessments, *51*. https://doi.org/10.1016/j.seta.2021.101912

Zhou, L., Hang, J., Bai, L., Krzemianowski, Z., El-Emam, M. A., Yasser, E., & Agarwal, R. (2022). Application of entropy production theory for energy losses and other investigation in pumps and turbines: A review. *Applied Energy*, *318*. https://doi.org/10.1016/j.apenergy.2022.119211